

Showcasing research from Professor Yamaguchi's laboratory, Institute of Transformative Bio-Molecules (ITbM), Nagoya University, Japan.

Near infrared two-photon-excited and -emissive dyes based on a strapped excited-state intramolecular proton-transfer (ESIPT) scaffold

2,5-Dithienylpyrrole-based fluorophores furnishing dialkylamine strap chains undergo the intramolecular proton transfer in the excited state, which gives rise to a significantly red-shifted emission. In addition, their acceptor- $\pi$ -donor- $\pi$ -acceptor structures render them being suitable for two-photon excitation. Consequently, the fluorophores can be excited by a near infrared (NIR) light and exhibit an intense emission in the NIR region.

As featured in:



See Daisuke Yokogawa, Kenji Kamada, Shigehiro Yamaguchi *et al.*, *Chem. Sci.*, 2018, 9, 2666.

Cite this: *Chem. Sci.*, 2018, 9, 2666

# Near infrared two-photon-excited and -emissive dyes based on a strapped excited-state intramolecular proton-transfer (ESIPT) scaffold†

Naoya Suzuki,<sup>a</sup> Kayo Suda,<sup>b</sup> Daisuke Yokogawa,<sup>c</sup> \*<sup>ab</sup> Hirotaka Kitoh-Nishioka,<sup>d</sup> <sup>a</sup> Stephan Irle,<sup>e</sup> <sup>ab</sup> Akihiro Ando,<sup>c</sup> Luis M. G. Abegão,<sup>cd</sup> Kenji Kamada,<sup>\*c</sup> Aiko Fukazawa,<sup>a</sup> <sup>a</sup> and Shigehiro Yamaguchi <sup>\*ab</sup>

Fluorophores that can undergo excited-state intramolecular proton transfer (ESIPT) represent promising scaffolds for the design of compounds that show red-shifted fluorescence. Herein, we disclose new near infrared-emissive materials based on a dialkylamine-strapped 2,5-dithienylpyrrole as an ESIPT scaffold. The introduction of electron-accepting units to the terminal positions of this scaffold generates acceptor- $\pi$ -donor- $\pi$ -acceptor (A- $\pi$ -D- $\pi$ -A) type  $\pi$ -conjugated compounds. Following the ESIPT, the electron-donating ability of the core scaffold increases, which results in a substantially red-shifted emission in the NIR region, while increasing the oscillator strength. The electron-accepting units play a vital role to achieve intense and red-shifted emission from the ESIPT state. The strapped dialkylamine chain that forms an intramolecular hydrogen bond is also essential to induce the ESIPT. Moreover, an extended A- $\pi$ -D- $\pi$ -A skeleton enables two-photon excitation with the NIR light. One of the derivatives that satisfy these features, *i.e.*, borylethenyl-substituted **5**, exhibited an intense NIR emission in polar solvents such as acetone ( $\lambda_{em} = 708$  nm,  $\Phi_F = 0.55$ ) with a strong two-photon-absorption band in the NIR region.

Received 7th January 2018  
Accepted 26th January 2018

DOI: 10.1039/c8sc00066b

rsc.li/chemical-science

## Introduction

Fluorescent molecules that exhibit emission in the near infrared (NIR) region have attracted increasing attention due to their versatile utility in biological applications<sup>1</sup> and optoelectronics.<sup>2,3</sup> In particular, the emission of such long-wavelength light reduces the phototoxicity toward cells, avoids interference from the auto-fluorescence background, and enables an in-depth penetration due to the low absorptivity between 650 nm and 900 nm in biological tissue.<sup>4</sup> Fluorophores with these features are highly desirable for optical imaging in biological research such as deep-tissue imaging.<sup>5</sup> Moreover, the

fabrication of organic light-emitting diodes using NIR fluorophores would provide a promising light source for various bio-sensing applications such as pulse oximeters.<sup>6</sup> Thus, considerable efforts have recently been devoted to the development of NIR fluorophores based on various design principles, such as construction of donor-acceptor-type skeletons,<sup>7-10</sup> modifications of polymethine-based skeletons such as cyanine dyes,<sup>11</sup> xanthene dyes,<sup>12-15</sup> and BODIPY,<sup>16,17</sup> as well as the formation of emissive excimers<sup>18</sup> or aggregates.<sup>19</sup> One particularly intriguing approach is based on the construction of a skeleton that features excited-state intramolecular proton transfer (ESIPT), *i.e.*, the intramolecular transfer of an acidic proton to a basic moiety in the excited state (ES).<sup>20</sup> Consequently, such a fluorophore can exhibit fluorescence with a large Stokes shift, which is the most notable feature of ESIPT-capable fluorophores compared to other types of emitting materials.

Various types of the ESIPT systems have been reported, *e.g.* those containing 2-hydroxyphenyl-substituted benzothiazoles,<sup>21</sup> benzoxazoles,<sup>21a,22</sup> imidazoles,<sup>23</sup> imidazo[1,2-*a*]pyridines,<sup>24,25</sup> or 10-hydroxy benzo[*h*]quinolines.<sup>26</sup> In particular, some ESIPT fluorophores with azole-type heterocycles have a suitable structure to avoid a nonradiative twisted intramolecular charge transfer process,<sup>27</sup> and thereby exhibit intense ESIPT emission in the visible region. However, ESIPT fluorophores often suffer from low fluorescence quantum yields when their emission

<sup>a</sup>Department of Chemistry, Graduate School of Science and Integrated Research Consortium on Chemical Sciences (IRCCS), Nagoya University, Japan

<sup>b</sup>Institute of Transformative Bio-Molecules (WPI-ITbM), Nagoya University, Furo, Chikusa, Nagoya, 464-8602, Japan

<sup>c</sup>IFMRI, National Institute of Advanced Industrial Science and Technology (AIST), 1-8-31 Midorigaoka, Ikeda, Osaka, 563-8577, Japan

<sup>d</sup>Departamento de Física, Universidade Federal de Sergipe, 49100-000 São Cristóvão, SE, Brazil

† Electronic supplementary information (ESI) available: Detailed synthetic protocols and characterization data of all new compounds, crystal structures of **3** and **6**, photophysical properties of **2**–**7**, details of theoretical calculations for **2** and **3**, including Schemes S1–S6 and Fig. S1–S83, and X-ray crystallographic data for **3** (CCDC 1813601) and **6** (CCDC 1813602). For ESI and crystallographic data in CIF or other electronic format see DOI: 10.1039/c8sc00066b



wavelengths reach the NIR region. One of the reasons for the inefficient ESIPT emission is slow radiative decay of the ES following proton transfer. Most conventional ESIPT systems rely on keto–enol tautomerism in the ES. This structural change results in a localization of the HOMO and LUMO in the ESIPT state, which results in a reduced overlap between ground and ES wavefunction and consequently leads to a small oscillator strength associated with the radiative decay.<sup>28</sup> In addition, according to the energy-gap law,<sup>29</sup> the nonradiative decay rate constants are expected to significantly increase upon bathochromically shifting the electronic transition. Therefore, a new design of an ESIPT-capable skeleton that does not rely on the keto–enol tautomerism is required to attain an intense emission in the NIR region based on the ESIPT mechanism.

Herein, we disclose a design strategy for fluorophores that exhibit a NIR-excited NIR emission based on a unique ESIPT skeleton. We have previously reported a 2,5-dithienylpyrrole that contains a dialkylamine strap as a core skeleton to induce ESIPT.<sup>30</sup> The underlying concept for the design of this scaffold is to introduce a basic amine moiety as a proton acceptor to an emissive  $\pi$ -conjugated skeleton with an acidic proton in a shape suitable for formation of an intramolecular hydrogen bond (Fig. 1a). Indeed, strapped 2,5-dithienylpyrrole **1**, which contains dimesitylboryl groups at the terminal positions, exhibited an emission band at  $\sim 600$  nm that was accompanied by a large Stokes shift in polar solvents, resulting from a zwitterionic ESIPT structure. Notably, a symmetric acceptor– $\pi$ -donor– $\pi$ -acceptor structure usually benefits efficient two-photon-absorption (TPA) properties.<sup>31</sup> This fact prompted us to aim at a more red-shifted NIR emission upon excitation with NIR light through TPA. To optimize the structure to this end, the key features should be (1) the electron-accepting ability of the terminal groups and (2) the hydrogen-bond-forming ability of the strap moiety. To explore the substituent effects, we synthesized a series of compounds **2–7** that contain various terminal groups and strap moieties (Fig. 1b). Among these,

compound **5**, which was extended with borylvinyl groups, indeed exhibited the desired bathochromically shifted NIR emission with high intensity.

## Results and discussion

### Synthesis of a series of strapped dithienylpyrroles

The synthesis of compounds **2–5** is shown in Scheme 1. Compounds **2** and **3** were synthesized in three steps from strapped dithienylpyrrole **8**. The pyrrole N–H moiety in **8** was initially protected with a *t*-butoxycarbonyl (Boc) group to afford **9**, which was transformed into **10** and **11** via lithiation with *n*-BuLi followed by treatment with the corresponding electrophiles. A subsequent heat-induced deprotection of the Boc group on the pyrrole afforded **2** and **3** as a colorless oil and a brown solid, respectively. Dimesitylborylyl-substituted **4** was synthesized in three steps from **9**. Namely, **9** was dilithiated with LDA, followed by treatment with 1,2-dibromotetrachloroethene to furnish **12**. After removal of the Boc group by treatment with an excess amount of sodium methoxide, Suzuki–Miyaura coupling reaction with the corresponding boron compound afforded **4** as a yellow powder. Dimesitylborylethenyl-substituted **5** was synthesized in three steps from **12**. Sonogashira–Hagihara coupling reaction between **12** and trimethylsilylacetylene afforded **13**, from which the trimethylsilyl and Boc groups were removed simultaneously by treatment with an excess amount of sodium methoxide to generate **14**. A subsequent hydroborylation with dimesitylborane afforded **5** as an orange powder. Reference compounds **6** and **7** with a longer or non-amine strapped chain, respectively, were synthesized in a similar manner as described for **3** and **5**, respectively.

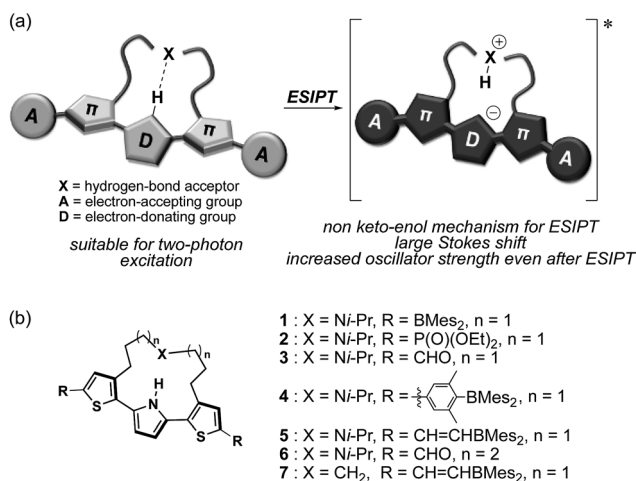
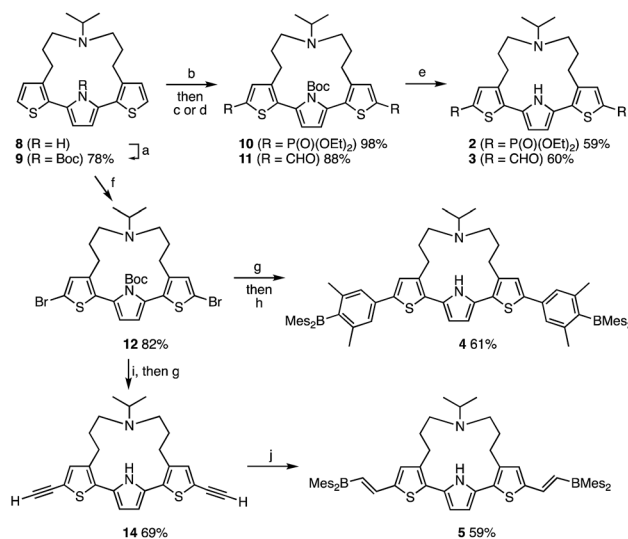


Fig. 1 (a) Schematic illustration of NIR two-photon-excited and -emissive strapped ESIPT dyes and (b) chemical structures of **1–7**, which were examined in this study.



Scheme 1 Synthesis of **2–5**. Reagents and conditions: (a) Boc<sub>2</sub>O, DMAP, MeCN, 80 °C; (b) *n*-BuLi, THF, –78 °C; (c) diethyl chlorophosphate, THF, –78 °C to rt; (d) DMF, THF, –78 °C to rt; (e) neat, 150 °C for **2**; 170 °C for **3**; (f) LDA, 1,2-dibromotetrachloroethane, THF, –78 °C to rt; (g) NaOMe, THF/MeOH, 80 °C; (h) 4-Mes<sub>2</sub>B-3,5-Me<sub>2</sub>-C<sub>6</sub>H<sub>2</sub>B(pin), Pd(PPh<sub>3</sub>)<sub>4</sub>, K<sub>2</sub>CO<sub>3</sub>, THF/H<sub>2</sub>O, 80 °C; (i) trimethylsilylacetylene, Pd(PPh<sub>3</sub>)<sub>4</sub>, CuI, *i*-Pr<sub>2</sub>NH, 70 °C; (j) HBMe<sub>2</sub>, THF, rt.



## The effect of terminal electron-accepting groups on the ESIPT behavior

Initially, we explored the impact of the terminal groups on the ESIPT behavior. For that purpose, we introduced diethoxy phosphoryl ( $-\text{P}(=\text{O})(\text{OEt})_2$ ) or formyl groups into **2** and **3**, respectively. Importantly, while the phosphoryl group can be considered as an electron-withdrawing group based on the inductive effect, the formyl group serves as an electron-accepting group that shows the mesomeric effect and participates in the delocalization of the LUMO (Fig. S22<sup>†</sup>). Consequently, **3** exhibits a much lower LUMO compared to that of **2**, and this difference is consistent with the photophysical properties of these compounds (Fig. 2a). The absorption spectrum of **3** in THF shows an absorption maximum ( $\lambda_{\text{abs}}$ ) at 423 nm, which is by 61 nm bathochromically shifted compared to that of **2**. The fluorescence spectra in the same solvent show an even more pronounced difference. While phosphoryl-substituted **2** exhibits an emission band ( $\lambda_{\text{em}}$ ) at 456 nm with shoulders at 420 nm and 487 nm, formyl-substituted **3** shows two distinct emission bands at 490 nm and 552 nm with Stokes shifts of  $3200\text{ cm}^{-1}$  and  $5500\text{ cm}^{-1}$ , respectively. Picosecond time-resolved fluorescence spectroscopy measurements showed that the fluorescence decay curves can be fitted with double-exponential functions for both compounds (**2**: 0.74 and 0.97 ns, **3**: 0.73 and 1.7 ns in THF, respectively. Fig. S12 and S13<sup>†</sup>), indicative of dual emission from the locally-excited (LE) and ESIPT states for both compounds. However, it is obvious that the ESIPT emission is more enhanced in formyl-substituted **3**. This difference implies that the degree of the electron-accepting ability of the terminal group should affect the acidity of the pyrrole N-H group in the ES.

Interestingly, **3** exhibited a distinct dependence of its dual emission properties on the solvent polarity (Fig. 2b). In nonpolar

cyclohexane, **3** exhibited an intense structured emission band at 466 nm ( $\Phi_{\text{F}} = 0.37$ ). The single exponential decay of the fluorescence suggests the existence of only LE state in this solvent. As the solvent polarity increases from benzene to THF to acetone, the emission band from the ESIPT state increased in intensity and was slightly red-shifted. Eventually, **3** showed emission only from the ESIPT state in acetone, as was evident from a single component of the fluorescence lifetime. It should be noted that the total fluorescence quantum yield increases with the solvent polarity and ultimately reaches  $\Phi_{\text{F}} = 0.60$  in acetone. This is opposite to the general trend observed for conventional A- $\pi$ -D- $\pi$ -A-type compounds, whose quantum yields tend to decrease with increasing solvent polarity. This trend should result from the higher fluorescence quantum yield for the ESIPT emission compared to that for the LE emission. The radiative ( $k_{\text{r}}$ ) and nonradiative ( $k_{\text{nr}}$ ) decay rate constants from both states were determined based on the  $\Phi_{\text{F}}$  and  $\tau$  values (Table S1<sup>†</sup>). While the  $k_{\text{r}}$  and  $k_{\text{nr}}$  values are  $0.41 \times 10^9\text{ s}^{-1}$  and  $0.70 \times 10^9\text{ s}^{-1}$  for the LE state in cyclohexane, the values for the ESIPT state in acetone are  $0.27 \times 10^9\text{ s}^{-1}$  and  $0.18 \times 10^9\text{ s}^{-1}$ , respectively. This comparison clearly shows that the non-radiative decay from the ESIPT state is retarded to a larger extent.

## The effect of the length of the strap chain on the ESIPT behavior

To induce ESIPT, an appropriate chain length of the strap moiety is also crucial. Compound **6** bears the longer strap chain and shows, in sharp contrast to **3**, only a single emission band even in polar solvents (Fig. 2a). Its emission band is located in a similar region to that of the LE band of **3**. Time-dependent fluorescence measurements revealed that **6** has only a single component of the fluorescence lifetime. These results demonstrate that **6** is ESIPT inert even though it contains a proton-accepting amine in the strap chain.

The behavioral difference between **3** and **6**, despite sharing an identical fluorophore skeleton, should be attributed to differences in the ability to form an intramolecular hydrogen bond between the pyrrole N-H bond and the amine moiety of the strap. To obtain clear-cut evidence for such intramolecular hydrogen bonds, the molecular structures of **3** and **6** in the crystalline state were determined (Fig. 3). In the single crystals, the dithienylpyrrole scaffold of **6** adopts an unsymmetrically twisted structure. The dihedral angle between the central pyrrole ring and the thiophene rings are  $27.9^\circ$  and  $54.4^\circ$ . In contrast, **3** exhibits a relatively coplanar structure with dihedral angles of  $25.2^\circ$  and  $17.9^\circ$ . This difference should be responsible for the slightly red-shifted absorption maxima of **3** ( $\lambda_{\text{abs,max}} = 423\text{ nm}$ ) compared to that of **6** ( $\lambda_{\text{abs,max}} = 393\text{ nm}$ ). More importantly, while the distance between the two nitrogen atoms N1 and N2 in **6** is  $5.21\text{ \AA}$ , that in **3** is  $2.83\text{ \AA}$ , which clearly demonstrates the existence of an intramolecular hydrogen bond.<sup>32</sup> This comparison shows that the chain length of the strap moiety is critical for the formation of an intramolecular hydrogen bond.

The  $^1\text{H NMR}$  spectra of **3** and **6** in  $\text{C}_6\text{D}_6$  revealed that this structural difference is retained in solution. While the

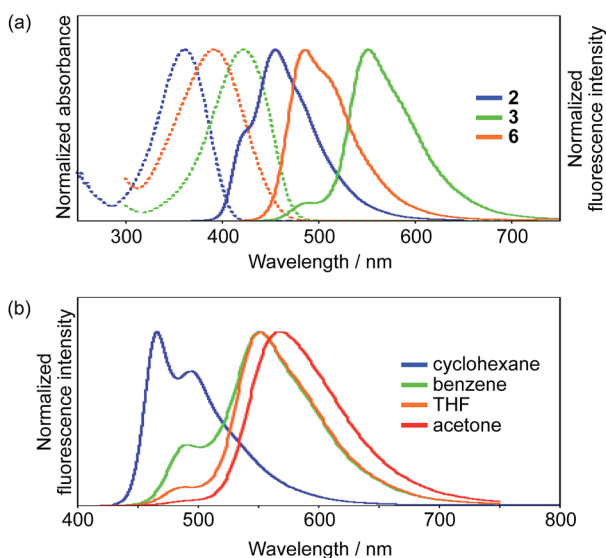


Fig. 2 UV-vis absorption and emission spectra of (a) **2**, **3**, and **6** in THF and (b) **3** in various solvents; dotted lines represent absorption, while solid lines show emission.



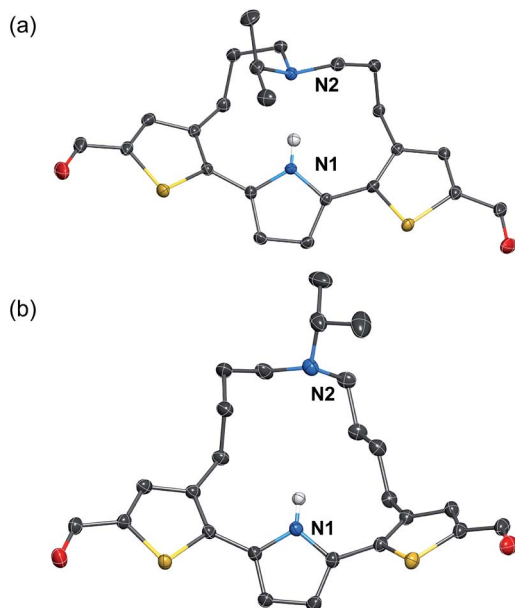


Fig. 3 X-ray crystal structures of (a) **3** and (b) **6** (thermal ellipsoids set to 50% probability). Expect for the N–H proton of the pyrrole ring, all hydrogen atoms are omitted for clarity.

resonance signal for the N–H proton of **6** appeared at 8.27 ppm, that of **3** was significantly downfield-shifted (13.1 ppm) (Fig. S1†). Comparisons of the ESIPT behavior and the structural features between **3** and **6** demonstrate that the pre-organization of the intramolecular hydrogen bond with a strap chain of appropriate chain length enables the efficient formation of the ESIPT state.

### Theoretical study of the ES

In comparison with conventional ESIPT systems that comprise 2-hydroxyphenyl-substituted azoles or related scaffolds, the most notable feature of our system is that intense emission is retained even in the ESIPT state. From this feature it can be inferred that even after the proton transfer occurs, the fluorophore skeleton retains the  $\pi$ -extended character of the A– $\pi$ –D– $\pi$ –A electronic structure. Moreover, in the ESIPT state, as the electron-donating character of the pyrrole moiety is enhanced, a quinoidal character with a more rigid planar structure is adopted, which could be the origin of the intense emission. For the theoretical elucidation of the ESIPT behavior in our system, **3** is the most suitable compound to investigate in depth, as it shows distinct emissions from the LE state in cyclohexane and from the ESIPT state in acetone. Based on this consideration, we conducted TD-DFT calculations on **3**, using the CAM-B3LYP functional in order to determine the structures in the LE and ESIPT states, where solvent effects were considered using the PCM model.

The geometry optimization of **3** in  $S_1$  revealed two local minima that can be associated with the LE and ESIPT states in both cyclohexane and acetone (Fig. 4). The relative energies of these two states strongly depend on the solvent polarity. In cyclohexane, the energies of the LE and ESIPT states relative to

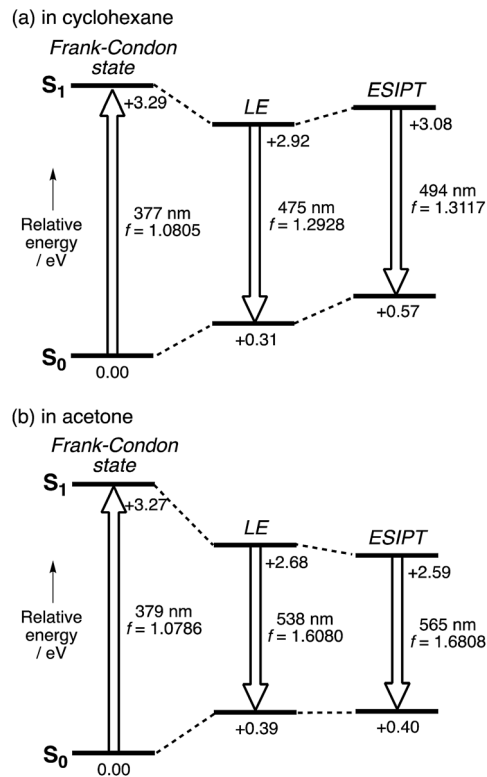


Fig. 4 Potential energy diagrams for **3** (a) in cyclohexane and (b) in acetone. The relative energies were calculated at the CAM-B3LYP/6-31+G(d) (N and O), 6-31G(d,p) (migrating H), and 6-31G(d) (all other atoms) levels of theory, and are given in eV relative to the optimized geometry in  $S_0$ .

the optimized structure in  $S_0$  are +2.92 eV and +3.08 eV. In contrast, the energies of both states decrease in acetone (LE: +2.68 eV; ESIPT: +2.59 eV), and, more importantly, the ESIPT state becomes thermodynamically more stable. These results are consistent with the experimentally observed solvent effect for **3**.

A notable characteristic of our strapped ESIPT system is the large oscillator strength ( $f$ ) of the electronic transition even in the ESIPT state. The  $f$  value of **3** for the LE state in cyclohexane (1.293) increases for the ESIPT state in acetone (1.681). As the radiative decay rate constant ( $k_r$ ) is proportional to the  $\nu^2 f$  value,<sup>33</sup> where  $\nu$  is discuss this  $\nu^2 f$  value. The calculated values for the LE state in cyclohexane ( $2.72 \times 10^{11} \text{ cm}^{-2}$ ) and the ESIPT state in acetone ( $2.97 \times 10^{11} \text{ cm}^{-2}$ ) are comparable to each other. This fact demonstrates that although the red-shift in the emission from the LE state in cyclohexane to the ESIPT state in acetone significantly decreases the  $\nu$  value, this is compensated by a concomitant increase in the oscillator strength in the ESIPT state by 30%. This is a rather unique feature of our system compared to conventional ESIPT systems.<sup>28</sup>

In addition, it is worth noting that the significant stabilization of the ESIPT state in acetone accompanies a substantial structural change. Fig. 5 shows the optimized geometry and plots of the variation in each bond distance from the ground state to the LE state in cyclohexane and the ESIPT state in



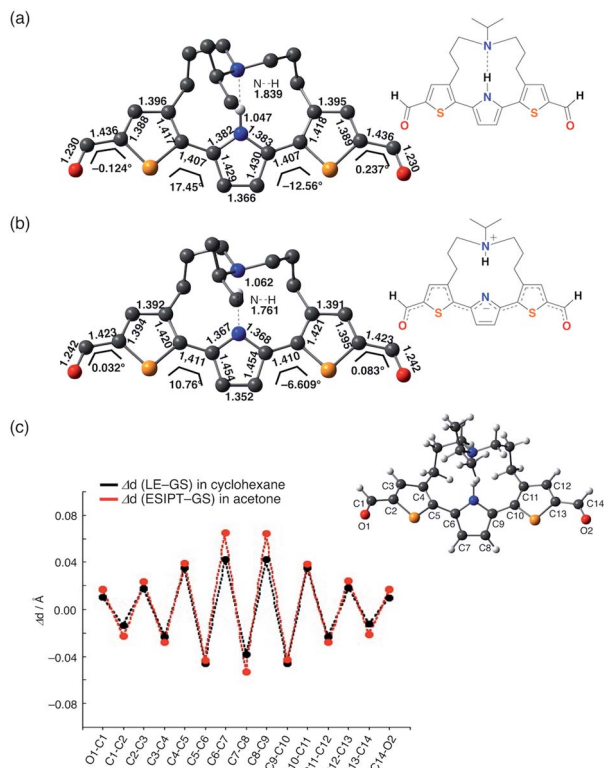


Fig. 5 Optimized geometries of **3** for (a) the LE state in cyclohexane and (b) the ES IPT state in acetone; (c) plots of the change in each bond distance during the structural relaxation in the ES and an atom-labeling scheme.

acetone. The larger structural relaxation in acetone than in cyclohexane leads to a more pronounced quinoidal character of the ES IPT state in acetone (Fig. 5c), where the C7–C8 bond is significantly shortened, and the C6–C7 and C8–C9 bonds in the central pyrrole ring are elongated. This structural change should be, at least in part, responsible for the increase in oscillator strength, and might also be relevant to the suppression of the non-radiative decay by forming a rigid planar quinoidal structure in the ES IPT state.

### Structural modifications to attain more red-shifted and brighter NIR emission

In order to achieve efficient ES IPT emission in the NIR region, we subsequently tried to expand the  $\pi$ -conjugation. Among **1–3**, dimesitylboryl-substituted **1** showed the longest-wavelength emission from the ES IPT state. Therefore, we used this scaffold and synthesized the corresponding  $\pi$ -extended derivatives **4** and **5**, which contain 3,5-dimethylphenyl and ethenyl groups between the thiophene and BMe<sub>2</sub> groups, respectively. Indeed, compounds **4** and **5** exhibited emission in the NIR region in polar solvents, whereby **4** showed a more pronounced response to the solvent polarity (Fig. 6). In cyclohexane, **4** exhibited an absorption band at 435 nm and a green fluorescence band at 513 nm with a Stokes shift of 3500 cm<sup>-1</sup>. In acetone, a significantly red-shifted ES IPT emission band appeared at 728 nm ( $\Phi_F = 0.18$ ). The Stokes shift reached 9600 cm<sup>-1</sup>, which is

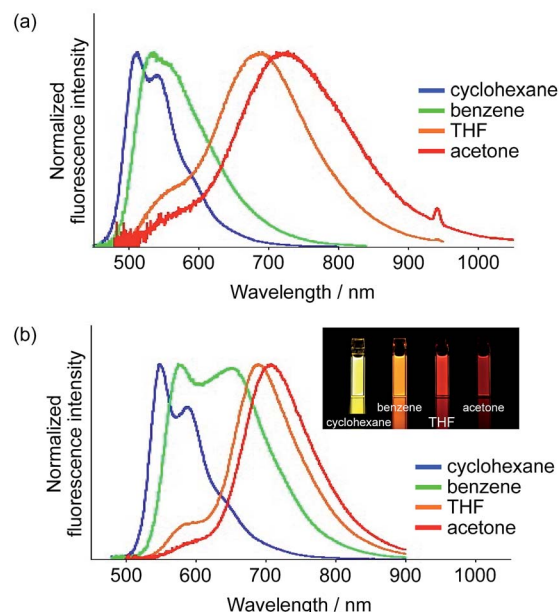


Fig. 6 Fluorescence spectra of (a) **4** and (b) **5** in various solvents (inset in b: photographs under irradiation with  $\lambda_{ex} = 365$  nm).

substantially larger than those of other derivatives, indicative of a large structural relaxation of **4** in polar solvents.

In terms of the fluorescence quantum yield, ethenyl-extended **5** exhibited more attractive properties. While **5** showed an intense emission at 547 nm from the LE state ( $\Phi_F = 0.68$ ) in cyclohexane, it exhibited NIR fluorescence from the ES IPT state in acetone at 708 nm with a Stokes shift of 6600 cm<sup>-1</sup>. Notably, the fluorescence quantum yield remained high ( $\Phi_F = 0.55$ ), despite the large Stokes shift. In light of the fact that examples of NIR-fluorescent ES IPT dyes with  $\lambda_{em} > 700$  nm and high fluorescence quantum yields are still limited,<sup>21g,34</sup> our system can be considered as a rather unique fluorescent scaffold.

### Two-photon absorption properties

It should also be noted that our system is beneficial to two-photon excitation. It has been well documented that A- $\pi$ -D-

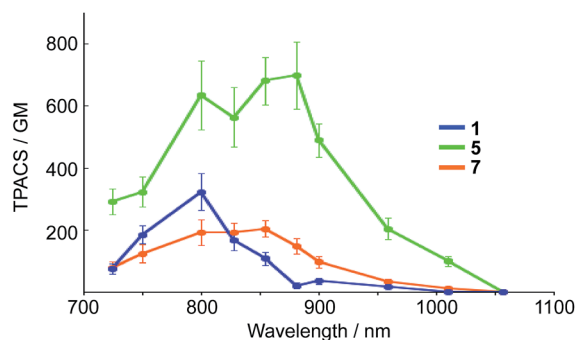


Fig. 7 Two-photon absorption cross section (TPACS) of **1**, **5**, and **7** in THF (solid circles). All data were corrected based on MPPBT/DMSO as the in-house standard.<sup>35</sup>



$\pi$ -A-type fluorophores exhibit a large two-photon absorption cross section (TPACS).<sup>31,35</sup> To assess this feature, we conducted TPA measurements on **5** together with **1** and **7** as reference compounds (Fig. 7). The TPA spectra were recorded in THF using the open-aperture Z-scan method with a femtosecond optical parametric amplifier (SpectraPhysics TOPAS Prime pumped by a Spitfire operating at a repetition rate of 1 kHz) as the light source by varying the incident wavelength. The results revealed that **5** exhibits the largest TPACS (698 GM at 881 nm), which is almost double that of boryl-substituted **1** (322 GM at 800 nm), which demonstrates the impact of the extension of the  $\pi$ -conjugation in **5**. This result also means that **5** can show an NIR emission at  $\sim$ 700 nm by two-photon excitation in the NIR region. It is the large Stokes shift of the ESIPT that can be the mechanism to achieve such a close energy difference between the emission and the two-photon excitation.

A comparison between **5** and **7** revealed the crucial role of the amine strap in **5** for its TPA properties. Compound **7**, which contains an alkyl chain strap instead of an amine, exhibited a TPACS value that was one third smaller than that of **5**, despite the fact that these compounds have the same  $\pi$ -conjugated scaffold. The temperature-dependent absorption spectra of **7** afforded insight into this difference (Fig. S21†). Compound **7** showed a broad absorption band at 300–550 nm at room temperature. Upon decreasing the temperature, the absorbance at 396 nm increased gradually, while that at 490 nm decreased with an isosbestic point. This spectral change indicates that **7** comprises two conformers in the ground state. The conformer exhibiting the absorption band at the longer wavelength, which most likely has a more planar structure, is thermodynamically less stable than the other. In sharp contrast, **5** only showed a single absorption band at 490 nm in solution. These differences suggest that the intramolecular hydrogen bond in **5** helps to constrain the conformation of the 2,5-dithienylpyrrole moiety in a planar fashion in the ground state. The population of the planar conformer is probably responsible for the increased TPACS of **5** compared to that of **7**.

## Conclusions

We have demonstrated that the nature of the terminal electron-accepting groups plays a crucial role for the ESIPT fluorescence properties of an alkylamine-strapped ESIPT chromophore based on 2,5-dithienylpyrrole. A diformyl derivative represents a suitable model to study the emission properties from the LE and ESIPT states. TD-DFT calculations revealed that in the ESIPT state the  $\pi$ -conjugated part of the molecule adopts a significant quinoidal structure. Of particular note is that a borylethenyl-substituted derivative **5** showed an intense NIR emission ( $\lambda_{\text{em}} = 708$  nm,  $\Phi_{\text{F}} = 0.55$ ) in acetone. Moreover, **5** can be excited by two-photon absorption, as it exhibits high two-photon absorption cross-section values. Notably, it is the ESIPT mechanism with a large Stokes shift that enables the close energy between the NIR two-photon excitation and the NIR emission. These features should offer significant merits in further applications of NIR fluorescent dyes, such as a deep-

tissue fluorescence imaging and NIR organic light-emitting diodes.

## Conflicts of interest

There are no conflicts to declare.

## Acknowledgements

This work was partly supported by JSPS KAKENHI grants 15H02163 (S. Y.), 24109007 and 25248007 (K. K.), and by a Grant-in-Aid for Scientific Research on Innovative Areas, Photosynergetics (JP26107004, K. K.) from MEXT, Japan, as well as by the Nagase Science and Technology Foundation and the Naito Foundation (S. Y.). ITbM is supported by the World Premier International Research Center (WPI) Initiative, Japan.

## Notes and references

- For recent reviews, see: (a) S. Luo, E. Zhang, Y. Su, T. Cheng and C. Shi, *Biomaterials*, 2011, **32**, 7127–7138; (b) V. Pansare, S. Hejazi, W. Faenza and R. K. Prud'homme, *Chem. Mater.*, 2012, **24**, 812–827; (c) X. Yi, F. Wang, W. Qin, X. Yang and J. Yuan, *Int. J. Nanomed.*, 2014, **9**, 1347–1365; (d) F. Anzengruber, P. Avci, L. Freitas de Freitas and M. R. Hamblin, *Photochem. Photobiol. Sci.*, 2015, **14**, 1492–1509; (e) G. Hong, A. L. Antaris and H. Dai, *Nature Biomedical Engineering*, 2017, **1**, 0010; (f) A. Haque, M. S. H. Faizi, J. A. Rather and M. S. Khan, *Bioorg. Med. Chem.*, 2017, **25**, 2017–2034.
- For reviews, see: (a) K.-Y. Law, *Chem. Rev.*, 1993, **93**, 449–486; (b) Y. Yang, Y. H. Zhang, W. Z. Shen and H. C. Liu, *Prog. Quantum Electron.*, 2011, **35**, 77–108.
- (a) N. Tessler, V. Medvedev, M. Kazes, S. Kan and U. Banin, *Science*, 2002, **295**, 1506–1508; (b) E. L. Williams, J. Li and G. E. Jabbour, *Appl. Phys. Lett.*, 2006, **89**, 083506; (c) D. Y. Kim, D. W. Song, N. Chopra, P. D. Somer and F. So, *Adv. Mater.*, 2010, **22**, 2260–2263; (d) J. Fischer, M. Tietke, F. Fritze, O. Muth, M. Paeschke, D. Han, J. Kwack, T. Kim, J. Lee, S. Kim and H. Chung, *J. Soc. Inf. Disp.*, 2011, **19**, 163–169; (e) B. Stender, S. F. Völker, C. Lambert and J. Pflaum, *Adv. Mater.*, 2013, **25**, 2943–2947; (f) P. A. Haigh, F. Bausi, Z. Ghassemlooy, I. Papakostantinou, H. L. Minh, C. Fléchon and F. Cacialli, *Opt. Express*, 2014, **22**, 2830–2838; (g) H. Tachibana, N. Aizawa, Y. Hidaka and T. Yasuda, *ACS Photonics*, 2017, **4**, 223–227.
- R. Weissleder, *Nat. Biotechnol.*, 2001, **19**, 316–317.
- (a) C. Bremer, C.-H. Tung and R. Weissleder, *Nat. Med.*, 2001, **7**, 743–748; (b) V. Ntziachristos, *Nat. Methods*, 2010, **7**, 603–614; (c) K. Welsch, S. P. Sherlock and H. Dai, *Proc. Natl. Acad. Sci. U. S. A.*, 2011, **108**, 8943–8948; (d) N. Zhang, K. P. Francis, A. Prakash and D. Ansaldi, *Nat. Med.*, 2013, **19**, 500–506; (e) D. M. Shcherbakova, M. Balaban, A. V. Emelyanov, M. Brenowitz, P. Guo and V. V. Verkhusha, *Nat. Commun.*, 2015, **7**, 12405.
- (a) C. M. Lochner, Y. Khan, A. Pierre and A. C. Arias, *Nat. Commun.*, 2014, **5**, 5745; (b) T. Yamanaka, H. Nakanotani,



- S. Hara, T. Hirohata and C. Adachi, *Appl. Phys. Express*, 2017, **10**, 074101.
- 7 (a) G. Qian, Z. Zhong, M. Luo, D. Yu, Z. Zhang, Z. Y. Wang and D. Ma, *Adv. Mater.*, 2009, **21**, 111–116; (b) A. L. Antaris, H. Chen, K. Cheng, Y. Sun, G. Hong, C. Qu, S. Diao, Z. Deng, X. Hu, B. Zhang, X. Zhang, O. K. Yaghi, Z. R. Alamparabli, X. Hong, Z. Cheng and H. Dai, *Nat. Mater.*, 2016, **15**, 235–242; (c) Y. Sun, C. Qu, H. Chen, M. He, C. Tang, K. Shou, S. Hong, M. Yang, Y. Jiang, B. Ding, Y. Xiao, L. Xing, X. Hong and Z. Cheng, *Chem. Sci.*, 2016, **7**, 6203–6207; (d) P. Murto, A. Minotto, A. Zampetti, X. Xu, M. R. Andersson, F. Cacialli and E. Wang, *Adv. Opt. Mater.*, 2016, **4**, 2068–2076; (e) Q. Yang, Z. Ma, H. Wang, B. Zhou, S. Zhu, Y. Zhang, J. Wang, H. Wan, A. Antaris, R. Ma, X. Zhang, J. Yang, X. Zhang, H. Sun, W. Liu, Y. Liang and H. Dai, *Adv. Mater.*, 2017, **29**, 1605497.
- 8 (a) A. Wakamiya, K. Mori and S. Yamaguchi, *Angew. Chem., Int. Ed.*, 2007, **46**, 4273–4276; (b) Z. Zhang, R. M. Edkins, J. Nitsch, K. Fucke, A. Steffen, L. E. Longobardi, D. W. Stephan, C. Lambert and T. B. Marder, *Chem. Sci.*, 2015, **6**, 308–321; (c) X. Yin, K. Liu, Y. Ren, R. A. Lalancette, Y.-L. Loo and F. Jäkle, *Chem. Sci.*, 2017, **8**, 5497–5505; (d) K. Liu, R. A. Lalancette and F. Jäkle, *J. Am. Chem. Soc.*, 2017, **139**, 18170–18173.
- 9 S. Wang, X. Yan, Z. Cheng, H. Zhang, Y. Liu and Y. Wang, *Angew. Chem., Int. Ed.*, 2015, **54**, 13068–13072.
- 10 M. Luo, H. Shadnia, G. Qian, X. Du, D. Yu, D. Ma, J. S. Wright and Z. Y. Wang, *Chem.–Eur. J.*, 2009, **15**, 8902–8908.
- 11 For recent reviews, see: (a) W. Sun, S. Guo, C. Hu, J. Fan and X. Peng, *Chem. Rev.*, 2016, **116**, 7768–7817; (b) C. Shi, J. B. Wu and D. Pan, *J. Biomed. Opt.*, 2016, **21**, 050901; (c) H. A. Shindy, *Dyes Pigm.*, 2017, **145**, 505–513.
- 12 For recent reviews, see: (a) Y.-Q. Sun, J. Liu, X. Lv, Y. Liu, Y. Zhao and W. Guo, *Angew. Chem., Int. Ed.*, 2012, **51**, 7634–7636; (b) Y. Kushida, T. Nagano and K. Hanaoka, *Analyst*, 2015, **140**, 685–695.
- 13 A. Fukazawa, J. Usuba, R. A. Alder and S. Yamaguchi, *Chem. Commun.*, 2017, **53**, 8565–8568.
- 14 (a) X. Chai, X. Cui, B. Wang, F. Yang, Y. Cai, Q. Wu and T. Wang, *Chem.–Eur. J.*, 2015, **21**, 16754–16758; (b) Y.-J. Gong, X.-B. Zhang, G.-J. Mao, L. Su, H.-M. Meng, W. Tan, S. Feng and G. Zhang, *Chem. Sci.*, 2016, **7**, 2275–2285; (c) X. Zhou, R. Lai, J. R. Beck, H. Li and C. I. Stains, *Chem. Commun.*, 2016, **52**, 12290–12293; (d) J. Liu, Y.-Q. Sun, H. Zhang, H. Shi, Y. Shi and W. Guo, *ACS Appl. Mater. Interfaces*, 2016, **8**, 22953–22962.
- 15 (a) M. V. Sednev, C. A. Wurm, V. N. Belov and S. W. Hell, *Bioconjugate Chem.*, 2013, **24**, 690–700; (b) A. Roth, H. Li, C. Anorma and J. Chan, *J. Am. Chem. Soc.*, 2015, **137**, 10890–10893; (c) M. Grzybowski, M. Taki and S. Yamaguchi, *Chem.–Eur. J.*, 2017, **23**, 13028–13032.
- 16 For recent reviews, see: (a) A. Loudet and K. Burgess, *Chem. Rev.*, 2007, **107**, 4891–4932; (b) Y. Ni and J. Wu, *Org. Biomol. Chem.*, 2014, **12**, 3774–3791.
- 17 (a) J. Bartelmess, M. Baldrighi, V. Nardone, E. Parisini, D. Buck, L. Echegoyen and S. Giordani, *Chem.–Eur. J.*, 2015, **21**, 9727–9732; (b) S. Cherumukkil, S. Ghosh, V. K. Praveen and A. Ajayaghosh, *Chem. Sci.*, 2017, **8**, 5644–5649; (c) A. Zampetti, A. Minotto, B. M. Squeo, V. G. Gregoriou, S. Allard, U. Scherf, C. L. Chochos and F. Cacialli, *Sci. Rep.*, 2017, **7**, 1611.
- 18 (a) C. Wei, M. Gao, F. Hu, J. Yao and Y. S. Zhao, *Adv. Opt. Mater.*, 2016, **4**, 1009–1014; (b) A. Jana, L. Bai, X. Li, H. Ågren and Y. Zhao, *ACS Appl. Mater. Interfaces*, 2016, **8**, 2336–2347.
- 19 (a) Q. Zhao, K. Li, S. Chen, A. Qin, D. Ding, S. Zhang, Y. Liu, B. Liu, J. Z. Sun and B. Z. Tang, *J. Mater. Chem.*, 2012, **22**, 15128–15135; (b) X. Du, J. Qi, Z. Zhang, D. Ma and Z. Y. Wang, *Chem. Mater.*, 2012, **24**, 2178–2185; (c) K. Cai, J. Xie and D. Zhao, *J. Am. Chem. Soc.*, 2014, **136**, 28–31; (d) G. M. Paternò, L. Moretti, A. J. Barker, C. D'Andrea, A. Luzio, N. Barbero, S. Galliano, C. Barolo, G. Lanzani and F. Scotognella, *J. Mater. Chem. C*, 2017, **5**, 7732–7738; (e) F. S. Freyria, J. M. Cordero, J. R. Caram, S. Doria, A. Dodin, Y. Chen, A. P. Willard and M. G. Bawendi, *Nano Lett.*, 2017, **17**, 7665–7674.
- 20 For recent reviews, see: (a) J. E. Kwon and S. Y. Park, *Adv. Mater.*, 2011, **23**, 3615–3642; (b) J. Zhao, S. Ji, Y. Chen, H. Guo and P. Yang, *Phys. Chem. Chem. Phys.*, 2012, **14**, 8803–8817; (c) A. P. Demochenko, K.-C. Tang and P.-T. Chou, *Chem. Soc. Rev.*, 2013, **42**, 1379–1408; (d) V. S. Padalkar and S. Seki, *Chem. Soc. Rev.*, 2016, **45**, 169–202.
- 21 (a) D. L. Williams and A. Heller, *J. Phys. Chem.*, 1970, **74**, 4473–4480; (b) K. Sakai, H. Kawamura, N. Kobayashi, T. Ishikawa, C. Ikeda, T. Kikuchi and T. Akutagawa, *CrystEngComm*, 2014, **16**, 3180–3185; (c) H.-W. Tseng, J.-Q. Liu, Y.-A. Chen, C.-M. Chao, K.-M. Liu, C.-L. Chen, T.-C. Lin, C.-H. Hung, Y.-L. Chou, T.-C. Lin, T.-L. Wang and P.-T. Chou, *J. Phys. Chem. Lett.*, 2015, **6**, 1477–1486; (d) W. Zhang, Y. Yan, J. Gu, J. Yao and Y. S. Zhao, *Angew. Chem., Int. Ed.*, 2015, **54**, 7125–7129; (e) P. Xu, T. Gao, M. Liu, H. Zhang and W. Zeng, *Analyst*, 2015, **140**, 1814–1816; (f) T. Gao, P. Xu, M. Liu, A. Bi, P. Hu, B. Ye, W. Wang and W. Zeng, *Chem.–Asian J.*, 2015, **10**, 1142–1145; (g) D. Dahal, L. McDonald, X. Bi, C. Abeywickrama, F. Gombedza, M. Konopka, S. Paruchuri and Y. Pang, *Chem. Commun.*, 2017, **53**, 3697–3700.
- 22 (a) C. H. Kim, J. Park, J. Seo, S. Y. Park and T. Joo, *J. Phys. Chem. A*, 2010, **114**, 5618–5629; (b) Y. Xu and Y. Pang, *Chem. Commun.*, 2010, **46**, 4070–4072; (c) K. Benelhadj, W. Muzuzu, J. Massue, P. Retailleau, A. Charaf-Eddin, A. D. Laurent, D. Jacquemin, G. Ulrich and R. Ziessel, *Chem.–Eur. J.*, 2014, **20**, 12843–12857.
- 23 (a) C. J. Fahrni, M. M. Henary and D. G. VanDerveer, *J. Phys. Chem. A*, 2002, **106**, 7655–7663; (b) M. M. Henary, Y. Wu, J. Cody, S. Sumalekshmy, J. Li, S. Mandal and C. J. Fahrni, *J. Org. Chem.*, 2007, **72**, 4784–4797; (c) S. Park, J. E. Kwon and S. Y. Park, *Phys. Chem. Chem. Phys.*, 2012, **14**, 8878–8884; (d) K. Skonieczny, J. Yoo, J. M. Larsen, E. M. Espinoza, M. Barbasiewicz, V. I. Vullev, C.-H. Lee and D. T. Gryko, *Chem.–Eur. J.*, 2016, **22**, 7485–7496.
- 24 For a recent review, see: A. J. Stasyuk, P. J. Cywiński and D. T. Gryko, *J. Photochem. Photobiol., C*, 2016, **28**, 116–137.





- 25 (a) H. Shono, T. Ohkawa, H. Tomoda, T. Mutai and K. Araki, *ACS Appl. Mater. Interfaces*, 2011, **3**, 654–657; (b) A. J. Stasyuk, M. Banasiewicz, M. K. Cyrański and D. T. Gryko, *J. Org. Chem.*, 2012, **77**, 5552–5558; (c) T. Mutai, H. Sawatani, T. Shida, H. Shono and K. Araki, *J. Org. Chem.*, 2013, **78**, 2482–2489; (d) A. J. Stasyuk, M. Banasiewicz, B. Ventura, M. K. Cyrański and D. T. Gryko, *New J. Chem.*, 2014, **38**, 189–197; (e) T. Mutai, T. Ohkawa, H. Shono and K. Araki, *J. Mater. Chem. C*, 2016, **4**, 3599–3606.
- 26 (a) E. L. Roberts, P. T. Chou, T. A. Alexander, R. A. Agbaria and I. M. Warner, *J. Phys. Chem.*, 1995, **99**, 5431–5437; (b) J. Piechowska and D. T. Gryko, *J. Org. Chem.*, 2011, **76**, 10220–10228; (c) J. Piechowska, K. Huttunen, Z. Wróbel, H. Lemmetyinen, N. V. Tkachenko and D. T. Gryko, *J. Phys. Chem. A*, 2012, **116**, 9614–9620; (d) K.-Y. Chen, H.-Y. Tsai, W.-C. Lin, H.-H. Chu, Y.-C. Weng and C.-C. Chan, *J. Chem. Sci.*, 2014, **126**, 955–966; (e) J. Piechowska, K. Virkki, B. Sadowski, H. Lemmetyinen, N. V. Tkachenko and D. T. Gryko, *J. Phys. Chem. A*, 2014, **118**, 144–151; (f) S. Hristova, G. Dobrikov, F. S. Kamounah, S. Kawauchi, P. E. Hansen, V. Deneva, D. Nedeltcheva and L. Antonov, *RSC Adv.*, 2015, **5**, 102495–102507; (g) H. Marciniak, S. Hristova, V. Deneva, F. S. Kamounah, P. E. Hansen, S. Lochbrunner and L. Antonov, *Phys. Chem. Chem. Phys.*, 2017, **19**, 26621–26629.
- 27 S. Kim, J. S. Seo and S. Y. Park, *J. Photochem. Photobiol., A*, 2007, **191**, 19–24.
- 28 (a) A. V. Gaenko, A. Devarajan, I. V. Tselinskii and U. Ryde, *J. Phys. Chem. A*, 2006, **110**, 7935–7942; (b) L. Xie, Y. Chen, W. Wu, H. Guo, J. Zhao and X. Yu, *Dyes Pigm.*, 2012, **92**, 1361–1369; (c) H. Roohi, F. Hejazi, N. Mohtamedifar and M. Jahantab, *Spectrochim. Acta, Part A*, 2014, **118**, 228–238; (d) R. Daengngern and N. Kungwan, *J. Lumin.*, 2015, **167**, 132–139; (e) I. Deperasińska, A. Makarewicz, M. Krzeszewski, D. T. Gryko and B. Kozankiewicz, *J. Phys. Chem. A*, 2015, **119**, 9051–9058.
- 29 (a) S. H. Lin, *J. Chem. Phys.*, 1970, **53**, 3766–3767; (b) J. V. Caspar, E. M. Kober, B. P. Sullivan and T. J. Meyer, *J. Am. Chem. Soc.*, 1982, **104**, 630–632; (c) J. V. Caspar and T. J. Meyer, *J. Phys. Chem.*, 1983, **87**, 952–957.
- 30 N. Suzuki, A. Fukazawa, K. Nagura, S. Saito, H. Kitoh-Nishioka, D. Yokogawa, S. Irlle and S. Yamaguchi, *Angew. Chem., Int. Ed.*, 2014, **53**, 8231–8235.
- 31 For a recent review, see: (a) M. Pawlicki, H. A. Collins, R. G. Denning and H. L. Anderson, *Angew. Chem., Int. Ed.*, 2009, **48**, 3244–3266; (b) Q. Zhang, X. Tian, H. Zhou, J. Wu and Y. Tian, *Materials*, 2017, **10**, 223.
- 32 For a review, see: T. Steiner, *Angew. Chem., Int. Ed.*, 2002, **41**, 48–76.
- 33 N. J. Turro, in *Modern Molecular Photochemistry*, University Science Books, Sausalito, CA, 1991, ch. 5, pp. 76–152.
- 34 (a) X. Cheng, K. Wang, S. Huang, H. Zhang, H. Zhang and Y. Wang, *Angew. Chem., Int. Ed.*, 2015, **54**, 8369–8373; (b) X. Cheng, Y. Zhang, S. Han, F. Li, H. Zhang and Y. Wang, *Chem.–Eur. J.*, 2016, **22**, 4899–4903; (c) R. Li, L. Yan, Z. Wang and Z. Qi, *J. Mol. Struct.*, 2017, **1136**, 1–6.
- 35 Y. Iwase, K. Kamada, K. Ohta and K. Kondo, *J. Mater. Chem.*, 2003, **13**, 1575–1581.

